ROYAL SOCIETY OF CHEMISTRY

PAPER

Check for updates

Aggregation state tuning *via* controlling molecular weights of D−A₁−A₂ type polymer donors for efficient organic photovoltaics†

Shanlu Wang,‡[a] Tianyi Chen,‡[a] Shuixing Li,*[a] Lei Ye,[b] Yuang Fu,[c] Xinhui Lu,[c] Haiming Zhu,[b] Lijian Zuo, [ID][a] Minmin Shi [ID][a] and Hongzheng Chen [ID]*[a]

Thiophene ring-based polymer donors generally face the challenges of high-lying energy levels and unfavorable aggregation states, thus limiting the performances of thiophene-based organic photovoltaics (OPVs). Herein, different from the traditional donor−acceptor (D−A) structure, we proposed a novel molecular design strategy of polymer donors by constructing a D−A₁−A₂ structure to achieve deep-lying energy levels, yielding PQC-TL, PQC-TM and PQC-TH, whose aggregation states in films could be controlled *via* molecular weights. A comparable study was performed by pairing these polymer donors with a newly synthesized monochlorinated non-fullerene acceptor L8-Cl. It's found that increasing the molecular weights of polymer donors leads to strengthened aggregation and reduced miscibility between the donor and acceptor, thus manipulating the domain sizes and crystallinity in polymer donor:L8-Cl blend films. An OPV device based on a PQC-TM donor with a medium molecular weight achieves a good balance between high crystallinity for efficient charge transport and suitable domain sizes for least charge recombination, thus enabling the highest efficiency of 15.0%, much higher than those (12.7% and 11.3%) of PQC-TL and PQC-TH-based devices. Anyway, this work demonstrates D−A₁−A₂ as a feasible molecular structure for designing efficient thiophene ring-based polymer donors and shows the critical role of molecular weight in controlling the aggregation state and device performance.

1 Introduction

Organic photovoltaics (OPVs) have increasingly attracted the interests of researchers due to their inherent advantages, such as light weight, solution processability, and flexible large-area manufacturing.[1–10] Owing to the continuous development of polymer donors and non-fullerene acceptors (NFAs), such as state-of-the-art Y-series molecules,[11–14] the power conversion efficiency (PCE) of OPVs has gradually exceeded 19%.[10,15–21] A key factor in determining the efficiencies of OPVs is the bulk-heterojunction (BHJ) blend morphology, which requires the formation of interpenetrating networks with suitable domain sizes and superior charge transport properties.[22–24] According to

intrinsic material properties, polymer donors play the main role in constructing the basic framework of an interpenetrating network *via* the temperature-dependent aggregation (TDA) behavior.[25–30] However, to obtain the optimized device performance, different TDA situations of polymer donors are required when pairing with varied electron acceptors. The preaggregation properties of a polymer donor, normally characterized by solution absorption change at varied temperatures, play an important role in affecting the domain sizes for balancing efficient charge separation and charge transport.[31–33] For example, to match small molecule NFAs normally featuring over-aggregation, polymer donors with strong solution preaggregation properties even at high temperatures, *e.g.*, PM6, are good choices, so as to tune the domain sizes for avoiding the over aggregation of NFAs.[34] For polymer acceptors that tend to over-mix with polymer donors, the preferred polymer donors should have medium aggregation ability, *e.g.*, PQM-Cl, so as to avoid over mixing for maintaining good domain purity.[30] Obviously, aggregation state turning of polymer donors plays a critical role in affecting the device performance.[35–38]

In the design of donor–acceptor (D–A) type polymer donors with TDA behavior, the benzodithiophene (BDT) unit is the most popularly used D building block but requires complex synthetic procedures. Relatively, the thiophene unit is a more economic D building block. Recently, thiophene rings as D

[a]*Department of Polymer Science and Engineering, State Key Laboratory of Silicon Materials, MOE Key Laboratory of Macromolecular Synthesis and Functionalization, Zhejiang University, Hangzhou 310027, P. R. China. E-mail: lishuixing89@163.com; hzchen@zju.edu.cn*

[b]*Department of Chemistry, Zhejiang University, Hangzhou 310027, P. R. China*

[c]*Department of Physics, Chinese University of Hong Kong, New Territories, Hong Kong 999077, P. R. China*

‡ S. Wang and T. Chen contributed equally to this work.

This journal is © The Royal Society of Chemistry 2023

J. Mater. Chem. A, 2023, 11, 6997–7005 | **6997**

building blocks also showed their potential in achieving high efficiencies.[39–43] Duan *et al.* reported that by combining a terpolymer with a ternary strategy, PCE over 17% could be realized in polythiophene derivative based OPVs.[42] On the other hand, the choices of A building blocks are diverse. When Y-series molecules became state-of-the-art NFAs, large π-conjugated electron-deficient units, such as dithieno[3′,2′:3,4;2″,3′′:5,6]benzo [1,2-c][1,2,5]thiadiazole (DTBT), emerged as outstanding units to construct polymer donors, such as D18.[44] Such large π-conjugated electron-deficient units not only help tune the TDA behavior, but also bring high luminescent properties, thus being a good choice as an A building block to design polymer donors.[37] The above two aspects inspire us to explore the possibility of combining a simple thiophene ring with a large π-conjugated electron-deficient unit for designing polymer donors and unveil the relationship between the aggregation state and device performance.

Generally, thiophene ring-based polymer donors will face the issue of high-lying energy levels, thus limiting the achievement of high voltage.[40] To solve such a problem, based on the traditional D–A structure, we here propose the combination of two different electron deficient units A_1 and A_2 as a whole "A" part to form D–A_1–A_2 type molecular structure arrangement. Herein,

ester functionalized thiophene[45–48] and dithieno[3,2-*f*:2′,3′-*h*] quinoxaline (DTQx) units[28,30] are selected as A_1 and A_2, respectively, and connected together as the whole electron-withdrawing part. After polymerizing the above whole electron-withdrawing part with a single thiophene ring, a novel wide bandgap polymer donor PQC-T was obtained and three different batches of PQC-T were synthesized with increased molecular weights of 22.0 kg mol^{-1}, 44.2 kg mol^{-1} and 59.1 kg mol^{-1}, which are then named PQC-TL, PQC-TM and PQC-TH, respectively, to perform a systematic study on how molecular weight affects the aggregation state of polymer donors and relevant device performance. And their molar-mass dispersities ($Đ_M = M_w/M_n$) were measured to be 2.44 for PQC-TL, 3.22 for PQC-TM and 3.08 for PQC-TH. It's unveiled that molecular weight is a critical factor in tuning the aggregation state of polymer donors, thus manipulating properties including the miscibility between the donor and acceptor, domain sizes, and crystallinity, finally having an effect on device performance. After optimization, an optimal PCE of 15.0% was achieved in PQC-TM:L8-Cl-based OPVs, representing D–A_1–A_2 as a feasible strategy for designing efficient thiophene ring-based polymer donors and the importance of controlling the molecular weight of polymer donors.
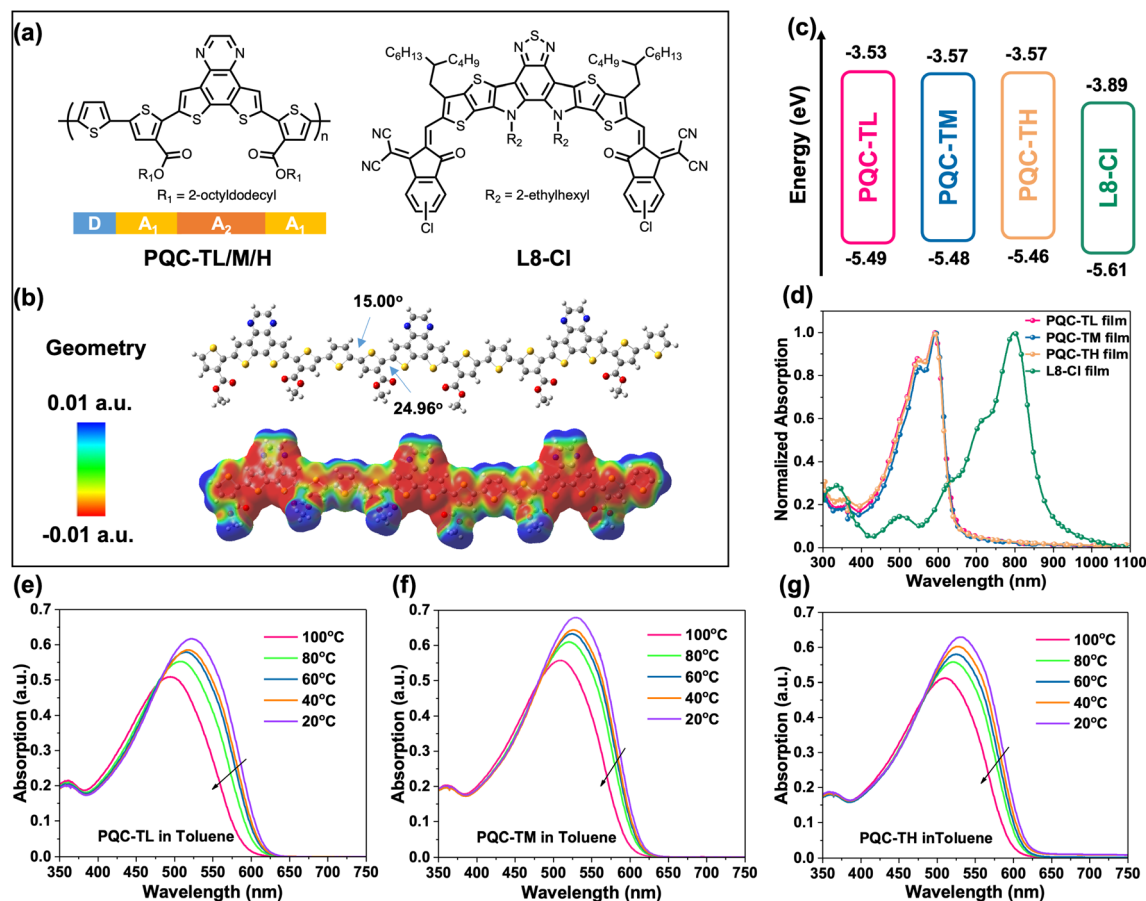

Fig. 1 (a) Molecular structures of PQC-TL/M/H and L8-Cl. (b) Geometric structures and ESP of trimer QC-T determined using DFT. (c) Energy level diagram of the donors and L8-Cl acceptor. (d) Normalized absorption spectra of the polymer donors and L8-Cl acceptor films. (e)–(g). Temperature-dependent absorption spectra of PQC-TL, PQC-TM, and PQC-TH in toluene.

6998 | *J. Mater. Chem. A*, 2023, **11**, 6997–7005

This journal is © The Royal Society of Chemistry 2023

2 Results and discussion

2.1. Synthesis and characterization

Fig. 1a shows the chemical structures of the designed D–A$_1$–A$_2$ type polymer donors, which are named PQC-TL, PQC-TM, PQC-TH, respectively, according to their varied molecular weights (22.0 kg mol^{-1} for PQC-TL, 44.2 kg mol^{-1} for PQC-TM, and 59.1 kg mol^{-1} for PQC-TH, Fig. S1†), and synthesized Y-series NFA L8-Cl for pairing with. The synthetic details of polymer donors and L8-Cl are described in the ESI.† Density functional theory (DFT) calculations were performed to obtain the geometry and electrostatic potential (ESP) information of the trimer for relevant polymer donors (Fig. 1b). It's found that such D–A$_1$–A$_2$ arrangement enables a planar backbone with dihedral angles of 15.00° between D and A$_1$ and 24.96° between A$_1$ and A$_2$. Besides, the main backbone of the trimer presents an overall negative ESP, reflecting its electron-donating properties as a donor (Fig. S2†).

To examine the effects of molecular weight on the photophysical properties of polymer donors, cyclic voltammetry (CV) measurement was first performed to check the energy levels (Fig. S3†). A gradual lift of the highest occupied molecular orbital (HOMO) level was observed from −5.49 eV to −5.48 eV, and then to −5.46 eV for PQC-TL, PQC-TM and PQC-TH with sequentially increased molecular weights. As for the lowest unoccupied molecular orbital (LUMO) level, PQC-TM and PQC-TH possess the same value of −3.57 eV, a bit deeper than that (−3.53 eV) of PQC-TL. Obviously, these three batches of polymer donors can match well with the NFA L8-Cl in energy levels (Fig. 1c).

Then absorption properties were studied to explore the aggregation state variation of these polymer donors (Fig. 1d and S4†). It's found that these three polymer donors have the same absorption edge of 651 nm in film, corresponding to an optical bandgap of 1.90 eV, complementary to the absorption of L8-Cl (Fig. S5†), but a stronger 0–0 peak and a narrower absorption window are presented for PQC-TM, indicating better molecular packing for PQC-TM. It's also well known that TDA behavior in solution is an important factor in the design of polymer donors.[49] We then checked temperature-dependent absorption spectra in toluene (0.0125 mg mL^{-1}) for these polymer donors (Fig. 1e–g). With the increase in temperature from 20 °C to 100 °C, PQC-TL undergoes the most obvious blue-shifting in absorption, representing strong preaggregation only at room temperature but not at high temperature, while PQC-TM shows the least blue-shifting in absorption, representing stronger preaggregation at both room temperature and high temperature. The above results indicate that molecular weight is a critical factor in tuning the aggregation state of polymer donors.

2.2. Photovoltaic properties

To investigate the photovoltaic performance of OPVs based on these three polymer donors and NFA L8-Cl, a conventional device architecture of ITO/PEDOT:PSS (poly(3,4-ethylenedioxythiophene) poly(styrene sulfonate))/active layer/PDINN/Ag was applied. The optimized conditions were found to be a D : A weight ratio of 1 : 1.2, the addition of 0.5% 1-chloronaphthalene (CN), and thermal annealing of 90 °C for 10 min (Tables S1–S3†). The champion J–V curves of the optimized devices are displayed in Fig. 2a, and the relevant
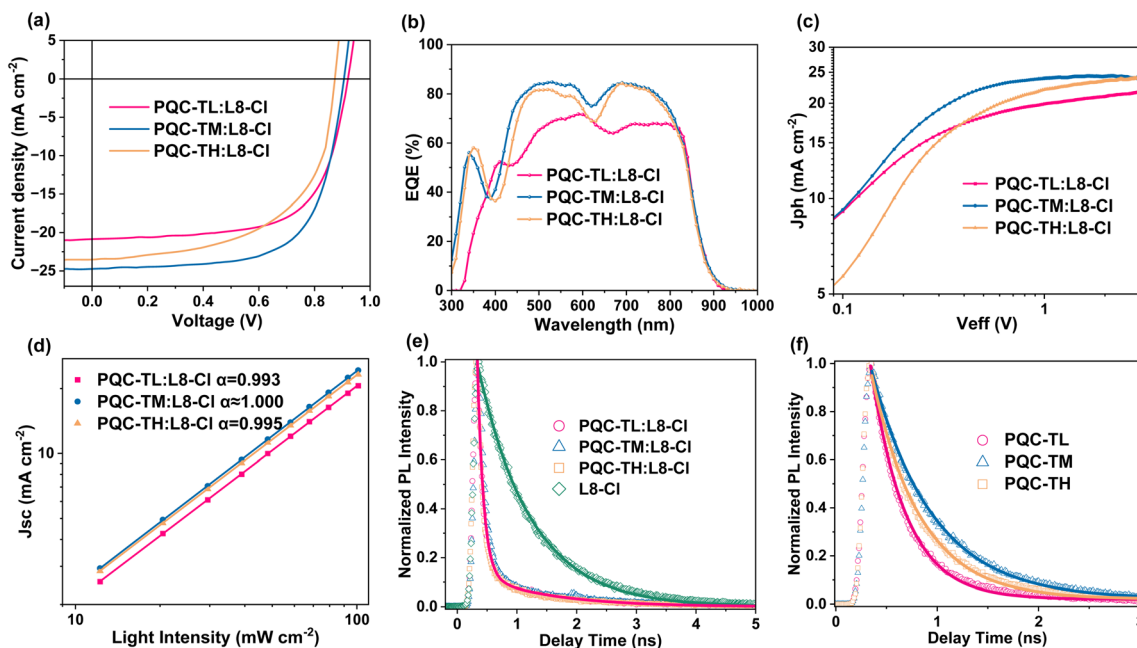

Fig. 2 (a) J−V characteristics, (b) EQE curves, (c) J_{ph}−V_{eff} curves, and (d) dependence of current density on light intensity of the OPVs based on PQC-TL:L8-Cl, PQC-TM:L8-Cl and PQC-TH:L8-Cl. (e) Time-resolved photoluminescence (TRPL) decay kinetics of PQC-TL:L8-Cl, PQC-TM:L8-Cl, PQC-TH:L8-Cl and L8-Cl films excited at 550 nm. (f) TRPL decay kinetics of PQC-TL, PQC-TM, and PQC-TH neat films excited at 550 nm.

Table 1 Photovoltaic parameters of optimized OPVs based on PQC-TL:L8-Cl, PQC-TM:L8-Cl and PQC-TH:L8-Cl blends

Blend	V_{OC}[a] (V)	J_{SC} (mA cm^{-2})	J_{cal}[b] (mA cm^{-2})	FF (%)	PCE (%)	E_{loss}[c] (eV)	R_s (Ω)	R_p (Ω)
PQC-TL:L8-Cl	0.921 (0.918 ± 0.002)	20.84 (20.53 ± 0.32)	20.00	66.06 (65.77 ± 0.41)	12.7 (12.4 ± 0.2)	0.48	131.92	62 158.71
PQC-TM:L8-Cl	0.906 (0.900 ± 0.003)	24.73 (24.53 ± 0.21)	23.93	67.05 (66.76 ± 0.50)	15.0 (14.7 ± 0.2)	0.49	115.64	23 757.46
PQC-TH:L8-Cl	0.889 (0.887 ± 0.003)	22.93 (22.69 ± 0.42)	22.85	55.31 (54.90 ± 0.61)	11.3 (11.0 ± 0.2)	0.51	166.49	8379.05

[a] Average values with standard deviation in brackets were acquired from at least ten independent devices. [b] Calculated current density from the EQE curve. [c] Energy loss calculated with the equation $E_{loss} = E_g - qV_{OC}$.

photovoltaic parameters are summarized in Table 1. With increasing molecular weight, a sequentially decreasing open-circuit voltage (V_{OC}) from 0.921 V to 0.906 V, and then to 0.889 V was observed for devices based on PQC-TL, PQC-TM and PQC-TH, which conform to the variations in the HOMO levels of these polymer donors. We then determined the energy loss (E_{loss}) values with the equation $E_{loss} = E_g - qV_{OC}$, in which E_g is determined using the absorption onset of narrower bandgap material, L8-Cl here (1.40 eV).[50,51] Correspondingly, E_{loss} values were calculated to be 0.48 eV, 0.49 eV and 0.51 eV for PQC-TL:L8-Cl, PQC-TM:L8-Cl, and PQC-TH:L8-Cl-based OPVs, respectively. The gradually increased energy loss might be attributed to the reduced offset between the HOMO level of the donor and LUMO level of the acceptor.

Besides the effect of V_{OC} on device performance, obvious differences are also present in the short-circuit current density (J_{SC}) and fill factor (FF). PQC-TM:L8-Cl-based OPVs demonstrated the highest J_{SC} of 24.73 mA cm^{-2} as well as the highest FF of 67.05%, thereby the highest PCE of 15.0%, while lower efficiencies of 12.7% and 11.3% were presented in PQC-TL:L8-Cl-based and PQC-TH:L8-Cl-based OPVs, respectively. As shown in Table 1, the lower series resistance (R_S) or higher parallel resistance (R_P) for the PQC-TL:L8-Cl-based device and PQC-TM:L8-Cl-based device could be the reason why these two devices possessed an obviously better FF than the PQC-TH:L8-Cl-based one.[52] The above results indicate that the molecular weight of a polymer donor plays a critical role in affecting the photovoltaic parameters, especially J_{SC} and FF.

External quantum efficiency (EQE) spectra were measured for cross-checking the photocurrent generation as detected in J–V curves. It's found that PQC-TM:L8-Cl-based and PQC-TH:L8-Cl-based devices show obvious higher photo-response in the broad range of 450–800 nm, thus enabling higher photocurrent than the PQC-TL:L8-Cl-based device, representing that a relatively high molecular weight is required for ensuring high photocurrent. The integrated current densities (J_{cal}) are found to be 20.00, 23.93 and 22.85 mA cm^{-2}, consistent with the J_{SC} values obtained from J–V curves.

Mobility properties were studied through the space-charge-limited current (SCLC) method by applying an architecture of ITO/PEDOT:PSS/active layer/MoO$_3$/Ag for hole-only devices and an architecture of ITO/ZnO/active layer/PDINN/Ag for electron-only devices, and the results are provided in Fig. S6 and Table S4.† The PQC-TM:L8-Cl-based device possesses the highest electron mobility of $10.14 × 10^{-5}$ cm^2 V^{-1} s^{-1} and also the most balanced hole/electron mobility ratio, which should be partly responsible for the achievement of higher J_{SC} and FF, relative to PQC-TL:L8-Cl-based and PQC-TH:L8-Cl-based devices.

To investigate the exciton dissociation and charge collection processes in the devices, the photocurrent density (J_{ph}) versus effective voltage (V_{eff}) curves were measured and the results are shown in Fig. 2c. The J_{ph} was determined using: $J_{ph} = J_L - J_D$, where J_L and J_D are the current density under light and dark conditions, respectively. V_{eff} is defined as $V_0 - V_{bias}$, where V_0 corresponds to the voltage where $J_{ph} = 0$ and V_{bias} is the applied voltage.[53] Here, saturation photocurrent density (J_{sat}) was reached when V_{eff} was ≈2.9 V for all devices. The OPVs based on PQC-TL:L8-Cl, PQC-TM:L8-Cl, and PQC-TH:L8-Cl blends showed P_{diss}/P_{coll} values of 90.77%/87.59%, 98.96%/96.92% and 90.46%/85.31%, respectively (Table S5†). Obviously, the PQC-TM:L8-Cl-based device presented the highest P_{diss}/P_{coll} values, indicating more efficient exciton dissociation and charge collection.[54] Thus, the PQC-TM:L8-Cl-based devices exhibited better performance.

Charge recombination situations were then examined by measuring the J–V curves at various light intensities (P_{light}) (see Fig. S7†). The relationship between J_{SC} and P_{light} is defined as $J_{SC} ∝ P_{light}{}^α$; a higher $α$ value means less bimolecular recombination.[55] As shown in Fig. 2d, $α$ values were calculated to be 0.993, 1.00 and 0.995 for PQC-TL:L8-Cl-based, PQC-TM:L8-Cl-based and PQC-TH:L8-Cl-based devices, respectively, which suggests less bimolecular recombination loss in the PQC-TM:L8-Cl-based devices. Furthermore, the relationship between V_{OC} and P_{light} can be defined as $V_{OC} ∝ nkT/q \ln(P_{light})$, where k, T, and q are the Boltzmann constant, absolute temperature and elementary charge, respectively. When the n value is close to 1, the bimolecular recombination is the major recombination pathway, while trap-assisted recombination dominates when the n value is close to 2.[56] As shown in Fig. S8,† the n values were 1.114, 1.109 and 1.234 kT/q for the devices based on PQC-TL:L8-Cl, PQC-TM:L8-Cl and PQC-TH:L8-Cl, respectively. The lowest n value demonstrated that the trap-assisted recombination was most efficiently suppressed in the PQC-TM-based device, which is well consistent with the higher charge carrier mobility and higher FF in the PQC-TM-based device. The more efficient exciton dissociation and charge collection, higher charge transport, and lower charge carrier recombination synergistically contribute to the better device performance of PQC-TM:L8-Cl-based OPVs.

To investigate the charge behavior in D:A blends, we measured time-resolved photoluminescence (TRPL) decay kinetics for neat and blend films and the results are shown in

7000 | J. Mater. Chem. A, 2023, **11**, 6997–7005

This journal is © The Royal Society of Chemistry 2023

Fig. 2e and f. Obviously, compared to the long PL lifetime of the L8-Cl neat film (0.886 ns), all three blends show similar shorter PL lifetimes of 0.103 ns, confirming the high exciton dissociation efficiency in D:A blends as discussed before. What's more, as depicted in Fig. 2f, the PQC-TM neat film reveals a longer PL lifetime (0.602 ns) than the PQC-TL (0.346 ns) and PQC-TH (0.481 ns) neat films, suggesting less defect state mediated charge recombination in the PQC-TM:L8-Cl blends,[57] which agrees well with the optimized charge recombination behaviors in PQC-TM:L8-Cl-based devices, and thus achieved a higher PCE.

2.3. Morphological analysis

Atomic force microscopy (AFM) was applied to investigate the surface morphological properties, and the results are depicted in Fig. S9.† With increasing molecular weight, the fibril feature becomes more and more obvious, especially for PQC-TH, implying improved crystallinity. In blend films, PQC-TM:L8-Cl shows the best bi-continuous interpenetrating network with the smallest root-mean-square (RMS) roughness of 0.89 nm, relative to PQC-TL:L8-Cl and PQC-TH:L8-Cl blends.

To further evaluate the detailed donor/acceptor phase segregation in the blend films of PQC-TL:L8-Cl, PQC-TM:L8-Cl, and PQC-TH:L8-Cl, we conducted the scanning near-field optical microscopy (SNOM) measurement.[38] For distinguishing the donor or acceptor components, we first measured the infrared (IR) absorption spectra of the donor and acceptor individually (Fig. S10†) and found correlative characteristic peaks at wavenumbers of 1712 cm^{-1} for PQC-T and 1531 cm^{-1}
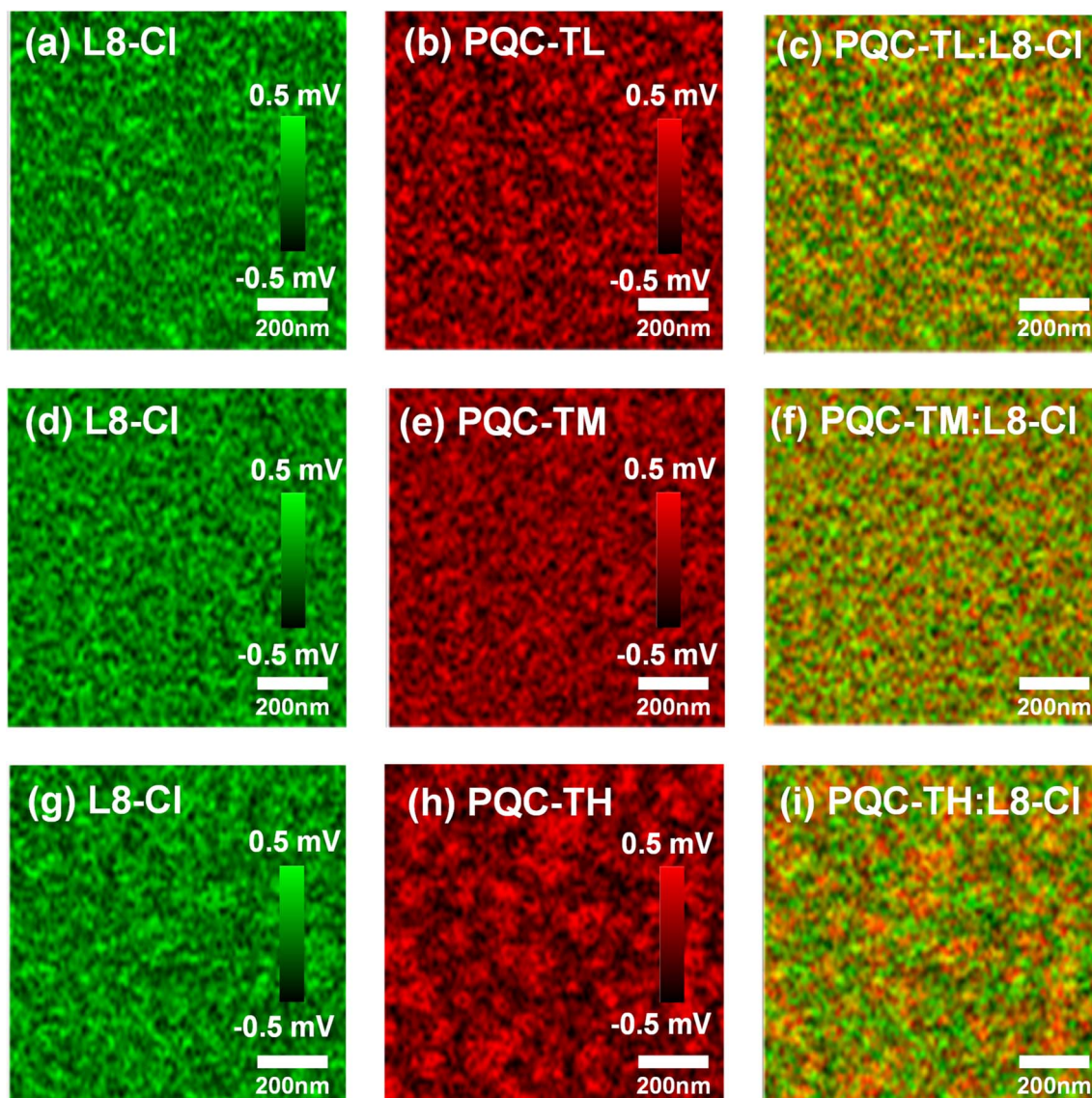

Fig. 3 SNOM images of the corresponding D:A blend films based on peaks at (a) 1531 cm^{-1} (L8-Cl component in the PQC-TL:L8-Cl blend), (b) 1712 cm^{-1} (PQC-TL component in the PQC-TL:L8-Cl blend), (d) 1531 cm^{-1} (L8-Cl component in the PQC-TM:L8-Cl blend), (e) 1712 cm^{-1} (PQC-TM component in the PQC-TM:L8-Cl blend), (g) 1531 cm^{-1} (L8-Cl component in the PQC-TH:L8-Cl blend), and (h) 1712 cm^{-1} (PQC-TH component in the PQC-TH:L8-Cl blend). (c) The combined image of (a) and (b) for the PQC-TL:L8-Cl blend. (f) The combined image of (d) and (e) for the PQC-TM:L8-Cl blend. (i) The combined image of (g) and (h) for the PQC-TH:L8-Cl blend.

This journal is © The Royal Society of Chemistry 2023

J. Mater. Chem. A, 2023, **11**, 6997–7005 | **7001**

for L8-Cl, respectively.[58] Then, combined with the AFM results, mapped SNOM images were obtained as shown in Fig. 3. Obviously, the PQC-TH:L8-Cl blend shows larger domain sizes than the PQC-TL:L8-Cl and PQC-TM:L8-Cl blends, which originated from the aggregation of polymer donor PQC-TH. Considering the increased crystallinity from PQC-TL:L8-Cl to PQC-TH:L8-Cl blends as indicated in AFM images (Fig. S9†), the PQC-TM:L8-Cl blend not only possesses high crystallinity, but also reserves suitable domain sizes in a reasonable range.
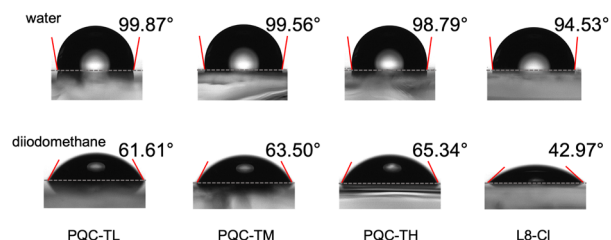

Fig. 4 Contact angle images of various films with water and diiodomethane droplets on top.

To explore the reasons causing the above phase separation situations, contact angle experiments were performed to study the miscibility between the donors and acceptor. The results can be found in Fig. 4 and Table 2. The miscibility properties between the donor and acceptor are characterized using the Flory–Huggins parameter (χ), and a higher value of χ represents a reduced miscibility.[59,60] It's found that the value of χ^{D-A} is increased from 0.88 for the PQC-TL:L8-Cl blend to 1.10 for the PQC-TM:L8-Cl blend, and then to 1.34 for PQC-TH:L8-Cl, indicating that higher molecular weight of a polymer donor will lead to lower miscibility with an acceptor, thus beneficial for higher crystallinity, finally resulting in various situations in domain sizes. However, overly large domain sizes should also be avoided for reducing monomolecular recombination as shown above.

Furthermore, grazing-incidence wide-angle X-ray scattering (GIWAXS) characterization was conducted to understand how the molecular weight of a polymer donor affects crystallinity and orientation.[61,62] The results are depicted in Fig. 5, S11 and Table S6.† For neat films, all three polymer donors adopt dominant face-on orientation with the π–π stacking peaks

Table 2 Surface free energy (SFE) characteristics of the neat films

Film	θ_{CH2I2} (°)	θ_{water} (°)	γ^d (mJ cm^{-2})	γ^p (mJ cm^{-2})	SFEγ (mJ cm^{-2})	$\chi^{D-A a}$
PQC-TL	61.61	99.87	27.06	0.68	27.74	0.88
PQC-TM	63.50	99.56	25.72	0.87	26.59	1.10
PQC-TH	65.34	98.79	24.31	1.20	25.51	1.34
L8-Cl	42.97	94.53	38.10	0.43	38.53	—

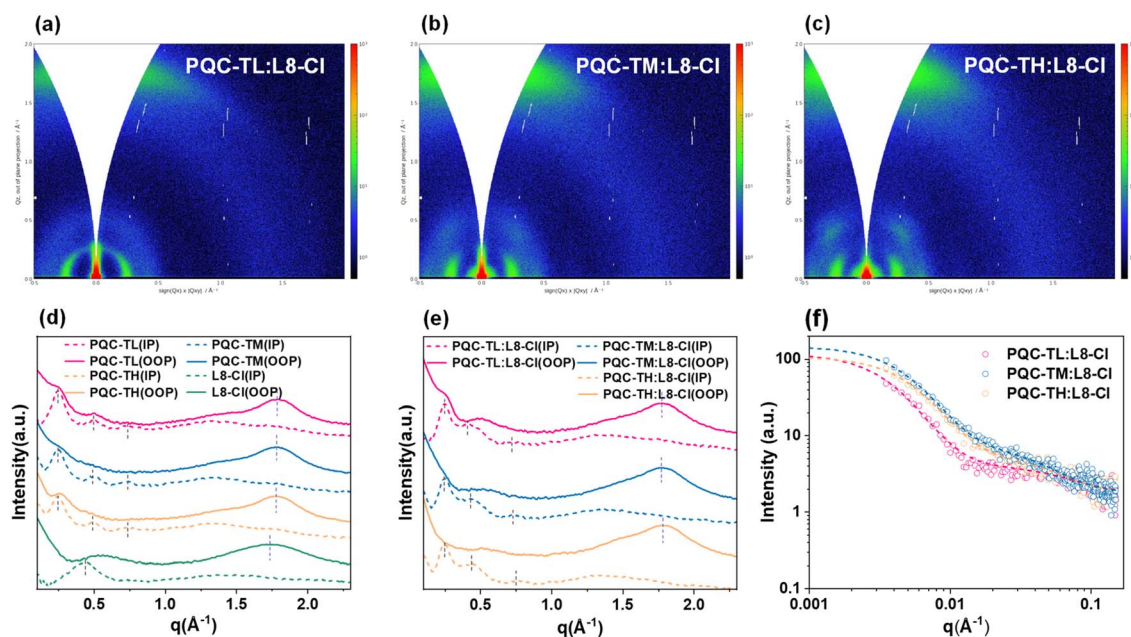^{a} $\chi^{D-A} = (\sqrt{\gamma_D} - \sqrt{\gamma_A})^2$.

Fig. 5 (a–c) 2D GIWAXS patterns of D:A blend films. (d–e) The corresponding intensity profiles along the out-of-plane (OOP) and in-plane (IP) directions extracted from 2D GIWAXS patterns.

7002 | *J. Mater. Chem. A*, 2023, **11**, 6997–7005

This journal is © The Royal Society of Chemistry 2023

located at 1.79 Å^{-1} ($d = 3.51$ Å) for PQC-TL and 1.78 Å^{-1} ($d = 3.53$ Å) for both PQC-TM and PQC-TH, respectively, in the out-of-plane (OOP) direction, while in the in-plane (IP) direction, besides the (100) lamellar peak at 0.25 Å^{-1} ($d = 25.12$ Å), both (200) and (300) high ordering diffraction peaks can be observed, representing high crystallinity for these three batches of polymer donors. In terms of crystallinity, PQC-TM and PQC-TH films are stronger than PQC-TL. As for the L8-Cl film, it also shows a face-on orientation with the π–π stacking peak located at 1.73 Å^{-1} ($d = 3.63$ Å). When polymer donors are blended with L8-Cl, face-on orientation is retained with the π–π stacking peaks at 1.77 Å^{-1} ($d = 3.55$ Å) for both PQC-TL:L8-Cl and PQC-TM:L8-Cl blends and 1.78 Å^{-1} ($d = 3.53$ Å) for the PQC-TH:L8-Cl blend. In terms of crystallinity, PQC-TM:L8-Cl and PQC-TH:L8-Cl blends possess higher crystallinity than the PQC-TL:L8-Cl blend, conforming to the results shown in AFM images. Besides, grazing-incidence small-angle X-ray scattering (GISAXS) measurement was also performed to detect whether varied aggregation states of polymer donors affect the acceptor domain sizes, and the results are displayed in Fig. 5f, S12 and Table S7.†[62] Although all three blend films show a similar size of pure acceptor domains, as indicated by their similar $2R_g$ values, the size of amorphous intermixed domains (X_{dab}) decreases monotonically from 21 nm to 14.7 nm with increasing M_n of polymer donors. This implies that the enhanced crystallinity of polymer donors suppresses the formation of intermixed domains, consistent with the suppressed recombination. Notably, the PQC-TM based system with a suitable degree of crystallinity and interfacial area achieves a balance between charge generation and transport, resulting in its superior J_{SC} and FF, and thus a highest PCE among the three blend systems studied. It can be seen that controlling molecular weights of polymer donors enables the tuning of the aggregation state and miscibility, thus resulting in various crystallinities and domain sizes. A suitable molecular weight polymer donor should be the one with a good balance between high crystallinity and suitable domain sizes.

3   Conclusions

In summary, we here propose a novel design of polymer donors with a D–A$_1$–A$_2$ type molecular structure, and three batches of polymer donors were synthesized with low, medium and high molecular weights, yielding PQC-TL, PQC-TM and PQC-TH, respectively. Besides, a monochlorinated NFA L8-Cl was also developed to pair with the designed polymer donors. It was found that aggregation states of polymer donors were well manipulated by controlling the molecular weight. A reduced miscibility between the donor and acceptor was achieved with increased molecular weights of polymer donors, due to which crystallinity and domain sizes were thereby regulated. PQC-TM with a medium molecular weight of 44.2 kg mol^{-1} was found to be a better choice in both maintaining high crystallinity for charge transport and forming suitable domain sizes for charge separation, relative to low molecular weight PQC-TL or high molecular weight PQC-TH. As a result, an optimal PCE of 15.0% was achieved in PQC-TM:L8-Cl-based OPVs, much higher than

those (12.7% and 11.3%) of PQC-TL:L8-Cl-based and PQC-TH:L8-Cl-based OPVs. This work not only demonstrates D–A$_1$–A$_2$ as a feasible molecular structure for designing polymer donors, but also verifies the critical role of molecular weight in aggregation state tuning of polymer donors.

Author contributions

S. Li and H. Chen conceived the idea. S. Wang designed the experiments and performed the chemical synthesis and property characterization of the polymer donors and acceptor. T. Chen performed the device fabrication, device measurements and data collection. L. Ye and H. Zhu contributed to the TRPL measurements and analysis. Y. Fu and X. Lu performed the GISAXS measurements and analysis. S. Wang drafted this paper. All the authors commented on the final paper. S. Li and H. Chen supervised the project.

Conflicts of interest

There are no conflicts to declare.

Acknowledgements

Notes and references

1 G. Li, R. Zhu and Y. Yang, *Nat. Photonics*, 2012, **6**, 153–161.
2 S. Li, W. Liu, C.-Z. Li, F. Liu, Y. Zhang, M. Shi, H. Chen and T. P. Russell, *J. Mater. Chem. A*, 2016, **4**, 10659–10665.
3 S. Li, W. Liu, C.-Z. Li, T.-K. Lau, X. Lu, M. Shi and H. Chen, *J. Mater. Chem. A*, 2016, **4**, 14983–14987.
4 S. Li, L. Zhan, F. Liu, J. Ren, M. Shi, C.-Z. Li, T. P. Russell and H. Chen, *Adv. Mater.*, 2018, **30**, 1705208.
5 W. Song, X. Fan, B. Xu, F. Yan, H. Cui, Q. Wei, R. Peng, L. Hong, J. Huang and Z. Ge, *Adv. Mater.*, 2018, **30**, 1800075.
6 L. Hong, H. Yao, Z. Wu, Y. Cui, T. Zhang, Y. Xu, R. Yu, Q. Liao, B. Gao, K. Xian, H. Y. Woo, Z. Ge and J. Hou, *Adv. Mater.*, 2019, **31**, 1903441.
7 L. Sun, W. Zeng, C. Xie, L. Hu, X. Dong, F. Qin, W. Wang, T. Liu, X. Jiang, Y. Jiang and Y. Zhou, *Adv. Mater.*, 2020, **32**, 1907840.
8 S. Li, L. Zhan, Y. Li, C. He, L. Zuo, M. Shi and H. Chen, *Small Methods*, 2022, **6**, 2200828.
9 X. Zheng, L. Zuo, F. Zhao, Y. Li, T. Chen, S. Shan, K. Yan, Y. Pan, B. Xu, C.-Z. Li, M. Shi, J. Hou and H. Chen, *Adv. Mater.*, 2022, **34**, 2200004.

This journal is © The Royal Society of Chemistry 2023

J. Mater. Chem. A, 2023, **11**, 6997–7005 | **7003**

10 L. Zhan, S. Yin, Y. Li, S. Li, T. Chen, R. Sun, J. Min, G. Zhou, H. Zhu, Y. Chen, J. Fang, C.-Q. Ma, X. Xia, X. Lu, H. Qiu, W. Fu and H. Chen, *Adv. Mater.*, 2022, **34**, 2206269.

11 R. Qin, D. Wang, G. Zhou, Z.-P. Yu, S. Li, Y. Li, Z.-X. Liu, H. Zhu, M. Shi, X. Lu, C.-Z. Li and H. Chen, *J. Mater. Chem. A*, 2019, **7**, 27632–27639.

12 C. He, Y. Li, Y. Liu, Y. Li, G. Zhou, S. Li, H. Zhu, X. Lu, F. Zhang, C.-Z. Li and H. Chen, *J. Mater. Chem. A*, 2020, **8**, 18154–18161.

13 S. Li, L. Zhan, Y. Jin, G. Zhou, T.-K. Lau, R. Qin, M. Shi, C.-Z. Li, H. Zhu, X. Lu, F. Zhang and H. Chen, *Adv. Mater.*, 2020, **32**, 2001160.

14 S. Li, L. Zhan, N. Yao, X. Xia, Z. Chen, W. Yang, C. He, L. Zuo, M. Shi, H. Zhu, X. Lu, F. Zhang and H. Chen, *Nat. Commun.*, 2021, **12**, 4627.

15 L. Zhu, M. Zhang, J. Xu, C. Li, J. Yan, G. Zhou, W. Zhong, T. Hao, J. Song, X. Xue, Z. Zhou, R. Zeng, H. Zhu, C.-C. Chen, R. C. I. MacKenzie, Y. Zou, J. Nelson, Y. Zhang, Y. Sun and F. Liu, *Nat. Mater.*, 2022, **21**, 656–663.

16 L. Zhan, S. Li, Y. Li, R. Sun, J. Min, Y. Chen, J. Fang, C.-Q. Ma, G. Zhou, H. Zhu, L. Zuo, H. Qiu, S. Yin and H. Chen, *Adv. Energy Mater.*, 2022, **12**, 2201076.

17 Y. Wei, Z. Chen, G. Lu, N. Yu, C. Li, J. Gao, X. Gu, X. Hao, G. Lu, Z. Tang, J. Zhang, Z. Wei, X. Zhang and H. Huang, *Adv. Mater.*, 2022, **34**, 2204718.

18 R. Sun, Y. Wu, X. Yang, Y. Gao, Z. Chen, K. Li, J. Qiao, T. Wang, J. Guo, C. Liu, X. Hao, H. Zhu and J. Min, *Adv. Mater.*, 2022, **34**, 2110147.

19 C. He, Y. Pan, Y. Ouyang, Q. Shen, Y. Gao, K. Yan, J. Fang, Y. Chen, C.-Q. Ma, J. Min, C. Zhang, L. Zuo and H. Chen, *Energy Environ. Sci.*, 2022, **15**, 2537–2544.

20 W. Gao, F. Qi, Z. Peng, F. R. Lin, K. Jiang, C. Zhong, W. Kaminsky, Z. Guan, C.-S. Lee, T. J. Marks, H. Ade and A. K. Y. Jen, *Adv. Mater.*, 2022, **34**, 2202089.

21 K. Chong, X. Xu, H. Meng, J. Xue, L. Yu, W. Ma and Q. Peng, *Adv. Mater.*, 2022, **34**, 2109516.

22 C. He, Y. Pan, G. Lu, B. Wu, X. Xia, C.-Q. Ma, Z. Chen, H. Zhu, X. Lu, W. Ma, L. Zuo and H. Chen, *Adv. Mater.*, 2022, **34**, 2203379.

23 C. He, Z. Chen, T. Wang, Z. Shen, Y. Li, J. Zhou, J. Yu, H. Fang, Y. Li, S. Li, X. Lu, W. Ma, F. Gao, Z. Xie, V. Coropceanu, H. Zhu, J.-L. Bredas, L. Zuo and H. Chen, *Nat. Commun.*, 2022, **13**, 2598.

24 K. Xian, K. Zhou, M. Li, J. Liu, Y. Zhang, T. Zhang, Y. Cui, W. Zhao, C. Yang, J. Hou, Y. Geng and L. Ye, *Chin. J. Chem.*, 2022, **41**, 159–166.

25 D. Qian, L. Ye, M. Zhang, Y. Liang, L. Li, Y. Huang, X. Guo, S. Zhang, Z. a. Tan and J. Hou, *Macromolecules*, 2012, **45**, 9611–9617.

26 Y. Liu, J. Zhao, Z. Li, C. Mu, W. Ma, H. Hu, K. Jiang, H. Lin, H. Ade and H. Yan, *Nat. Commun.*, 2014, **5**, 5293.

27 Z. Wang, Z. Peng, Z. Xiao, D. Seyitliyev, K. Gundogdu, L. Ding and H. Ade, *Adv. Mater.*, 2020, **32**, 2005386.

28 Y. Cui, Y. Xu, H. Yao, P. Bi, L. Hong, J. Zhang, Y. Zu, T. Zhang, J. Qin, J. Ren, Z. Chen, C. He, X. Hao, Z. Wei and J. Hou, *Adv. Mater.*, 2021, **33**, 2102420.

29 S. Wang, Y. Tao, S. Li, X. Xia, Z. Chen, M. Shi, L. Zuo, H. Zhu, X. Lu and H. Chen, *Macromolecules*, 2021, **54**, 7862–7869.

30 J. Wang, Y. Cui, Y. Xu, K. Xian, P. Bi, Z. Chen, K. Zhou, L. Ma, T. Zhang, Y. Yang, Y. Zu, H. Yao, X. Hao, L. Ye and J. Hou, *Adv. Mater.*, 2022, **34**, 2205009.

31 F. Panzer, M. Sommer, H. Bässler, M. Thelakkat and A. Köhler, *Macromolecules*, 2015, **48**, 1543–1553.

32 H. Kang, M. A. Uddin, C. Lee, K.-H. Kim, T. L. Nguyen, W. Lee, Y. Li, C. Wang, H. Y. Woo and B. J. Kim, *J. Am. Chem. Soc.*, 2015, **137**, 2359–2365.

33 B. Du, J. Yi, H. Yan and T. Wang, *Chem.–Eur. J.*, 2021, **27**, 2908–2919.

34 S. Zhang, Y. Qin, J. Zhu and J. Hou, *Adv. Mater.*, 2018, **30**, 1800868.

35 C. Sun, F. Pan, B. Qiu, S. Qin, S. Chen, Z. Shang, L. Meng, C. Yang and Y. Li, *Chem. Mater.*, 2020, **32**, 3254–3261.

36 X. Guo, Q. Fan, J. Wu, G. Li, Z. Peng, W. Su, J. Lin, L. Hou, Y. Qin, H. Ade, L. Ye, M. Zhang and Y. Li, *Angew. Chem., Int. Ed.*, 2021, **60**, 2322–2329.

37 Y. Xu, Y. Cui, H. Yao, T. Zhang, J. Zhang, L. Ma, J. Wang, Z. Wei and J. Hou, *Adv. Mater.*, 2021, **33**, 2101090.

38 C. Zhu, L. Meng, J. Zhang, S. Qin, W. Lai, B. Qiu, J. Yuan, Y. Wan, W. Huang and Y. Li, *Adv. Mater.*, 2021, **33**, 2100474.

39 C. Sun, F. Pan, H. Bin, J. Zhang, L. Xue, B. Qiu, Z. Wei, Z.-G. Zhang and Y. Li, *Nat. Commun.*, 2018, **9**, 743.

40 B. Yin, Z. Chen, S. Pang, X. Yuan, Z. Liu, C. Duan, F. Huang and Y. Cao, *Adv. Energy Mater.*, 2022, **12**, 2104050.

41 B. Yin, S. Pang, Z. Chen, W. Deng, Z. Liu, C. Duan, F. Huang and Y. Cao, *Energy Environ. Sci.*, 2022, **15**, 4789–4797.

42 X. Yuan, Y. Zhao, D. Xie, L. Pan, X. Liu, C. Duan, F. Huang and Y. Cao, *Joule*, 2022, **6**, 647–661.

43 X. Yuan, Y. Zhao, Y. Zhang, D. Xie, W. Deng, J. Li, H. Wu, C. Duan, F. Huang and Y. Cao, *Adv. Funct. Mater.*, 2022, **32**, 2201142.

44 Q. Liu, Y. Jiang, K. Jin, J. Qin, J. Xu, W. Li, J. Xiong, J. Liu, Z. Xiao, K. Sun, S. Yang, X. Zhang and L. Ding, *Sci. Bull.*, 2020, **65**, 272–275.

45 S. Li, L. Ye, W. Zhao, H. Yan, B. Yang, D. Liu, W. Li, H. Ade and J. Hou, *J. Am. Chem. Soc.*, 2018, **140**, 7159–7167.

46 H. Yao, Y. Cui, D. Qian, C. S. Ponseca Jr, A. Honarfar, Y. Xu, J. Xin, Z. Chen, L. Hong, B. Gao, R. Yu, Y. Zu, W. Ma, P. Chabera, T. Pullerits, A. Yartsev, F. Gao and J. Hou, *J. Am. Chem. Soc.*, 2019, **141**, 7743–7750.

47 Y. Zhang, D. Liu, T.-K. Lau, L. Zhan, D. Shen, P. W. K. Fong, C. Yan, S. Zhang, X. Lu, C.-S. Lee, J. Hou, H. Chen and G. Li, *Adv. Funct. Mater.*, 2020, **30**, 1910466.

48 S. Huang, W. Gu, L. Chen, Z. Liao, Y. An, C. An, Y. Chen and J. Hou, *Macromol. Rapid Commun.*, 2019, **40**, 1800906.

49 H. Hu, P. C. Y. Chow, G. Zhang, T. Ma, J. Liu, G. Yang and H. Yan, *Acc. Chem. Res.*, 2017, **50**, 2519–2528.

50 X. Ma, A. Zeng, J. Gao, Z. Hu, C. Xu, J. H. Son, S. Y. Jeong, C. Zhang, M. Li, K. Wang, H. Yan, Z. Ma, Y. Wang, H. Y. Woo and F. Zhang, *Natl. Sci. Rev.*, 2021, **8**, nwaa305.

51 C. Xu, K. Jin, Z. Xiao, Z. Zhao, X. Ma, X. Wang, J. Li, W. Xu, S. Zhang, L. Ding and F. Zhang, *Adv. Funct. Mater.*, 2021, **31**, 2107934.

7004 | *J. Mater. Chem. A*, 2023, **11**, 6997–7005

This journal is © The Royal Society of Chemistry 2023

52 S. Zhang, X. Ma, L. Niu, S. Y. Jeong, H. Y. Woo, Z. Zhou and F. Zhang, *Sol. RRL*, 2023, **7**, 2200957.

53 P. W. M. Blom, V. D. Mihailetchi, L. J. A. Koster and D. E. Markov, *Adv. Mater.*, 2007, **19**, 1551–1566.

54 L. Zhan, S. Li, X. Xia, Y. Li, X. Lu, L. Zuo, M. Shi and H. Chen, *Adv. Mater.*, 2021, **33**, 2007231.

55 V. Gupta, A. K. K. Kyaw, D. H. Wang, S. Chand, G. C. Bazan and A. J. Heeger, *Sci. Rep.*, 2013, **3**, 1965.

56 L. J. A. Koster, V. D. Mihailetchi, R. Ramaker and P. W. M. Blom, *Appl. Phys. Lett.*, 2005, **86**, 123509.

57 Z. Chen, X. Chen, Z. Jia, G. Zhou, J. Xu, Y. Wu, X. Xia, X. Li, X. Zhang, C. Deng, Y. Zhang, X. Lu, W. Liu, C. Zhang, Y. Yang and H. Zhu, *Joule*, 2021, **5**, 1832–1844.

58 J. Jahng, D. A. Fishman, S. Park, D. B. Nowak, W. A. Morrison, H. K. Wickramasinghe and E. O. Potma, *Acc. Chem. Res.*, 2015, **48**, 2671–2679.

59 L. Ye, H. Hu, M. Ghasemi, T. Wang, B. A. Collins, J.-H. Kim, K. Jiang, J. H. Carpenter, H. Li, Z. Li, T. McAfee, J. Zhao, X. Chen, J. L. Y. Lai, T. Ma, J.-L. Bredas, H. Yan and H. Ade, *Nat. Mater.*, 2018, **17**, 253–260.

60 M. Ghasemi, N. Balar, Z. Peng, H. Hu, Y. Qin, T. Kim, J. J. Rech, M. Bidwell, W. Mask, I. McCulloch, W. You, A. Amassian, C. Risko, B. T. O'Connor and H. Ade, *Nat. Mater.*, 2021, **20**, 525–532.

61 J. Rivnay, S. C. B. Mannsfeld, C. E. Miller, A. Salleo and M. F. Toney, *Chem. Rev.*, 2012, **112**, 5488–5519.

62 P. Müller-Buschbaum, *Adv. Mater.*, 2014, **26**, 7692–7709.

This journal is © The Royal Society of Chemistry 2023

J. Mater. Chem. A, 2023, **11**, 6997–7005 | **7005**